

## Sulfolipid density dictates the extent of carbon nanodot interaction with chloroplast membranes

Kyoungtea Kim,<sup>a,1</sup> Su-Ji Jeon,<sup>b</sup> Peiguang Hu,<sup>b,2</sup> Caroline M. Anastasia,<sup>c</sup> William F. Beimers,<sup>d,3</sup> Juan Pablo Giraldo,<sup>\*,b</sup> and Joel A. Pedersen<sup>\*,a,c,e,4</sup>

<sup>a</sup> Molecular and Environmental Toxicology, University of Wisconsin—Madison, Madison, Wisconsin 53706, United States

<sup>b</sup> Department of Botany and Plant Sciences, University of California—Riverside, Riverside, California 92521, United States

<sup>c</sup> Department of Chemistry, University of Wisconsin—Madison, Madison, Wisconsin 53706, United States

<sup>d</sup> Department of Chemistry, St. Olaf College, Northfield, Minnesota 55057, United States

<sup>e</sup> Departments of Soil Science and Civil & Environmental Engineering, University of Wisconsin—Madison, Madison, Wisconsin 53706, United States

<sup>1</sup> Present address: Eshelman School of Pharmacy, University of North Carolina at Chapel Hill, Chapel Hill, North Carolina 27599, United States

<sup>2</sup> Present address: Westwood Bioscience, Los Angeles, California 90025, United States

<sup>3</sup> Present address: Department of Biochemistry, University of Wisconsin—Madison, Madison, Wisconsin 53706, United States

<sup>4</sup> Present address: Department of Environmental Health and Engineering, Johns Hopkins University, Baltimore, Maryland 21218, United States

## TABLE OF CONTENTS

### Methods

**Figure S1.** Removal of fluorescent by-products from synthesized CNDs.

**Figure S2.** X-ray photoelectron spectroscopy (XPS) analysis of PEI-, CP-, and PVP-CNDs.

**Figure S3.** A representative QCM-D traces for model membrane construction and its interaction with CNDs

**Figure S4.** Association of PEI-, CP-, and PVP-CNDs with model membranes containing 5% SQDG under 0-100 mM KCl buffered to pH 7.5 with 10 mM HEPES

**Figure S5.** Calculated dissipation changes per unit adsorbed mass ( $\Delta D/\Delta f$ ) upon the interaction with the PEI-CNDs.

**Figure S6.** Mass densities upon PEI-CND exposure on 0%, 2.5%, and 10% SQDG containing model membranes

**Figure S7.** Representative confocal images of isolated chloroplasts without exposure to PEI-CNDs.

**Figure S8.** Representative TEM images of bare CNDs.

**Table S1.** Ratio of SQDG to PEI-CND at the maximum adsorption of CNDs

## METHODS

**Cleaning of Used Sensors and QCM-D Flow Cells.** Used sensors were cleaned as described previously.<sup>1</sup> Briefly, after each measurement, used SiO<sub>2</sub> QCM-D sensors were briefly rinsed with ultrapure water flow and immersed in 2 wt. % SDS solution for 30 min at room temperature. Afterward, the immersed sensors were sonicated for 5 min in a bath sonicator followed by a rinse with ultrapure water. The rinsed sensor surfaces were dried with a stream of nitrogen gas and subjected to UV/ozone treatment for 10 min. For the cleaning process, sensor surfaces were kept wet until they were dried with a stream of nitrogen gas. Flow cells of QCM-D were cleaned with 2 wt. % SDS solution, Cobas cleaner solution (Roche, Basel, Switzerland), and 2 v/v % Hellmanex II solution (Hellma GmbH & Co. KG, Müllheim, Germany) at a flow rate of 200  $\mu\text{L}\cdot\text{min}^{-1}$  for 20 min, respectively. Cleaned flow cells were rinsed with ultrapure water flow for another 20 min at the same flow rate and dried with nitrogen gas flow.

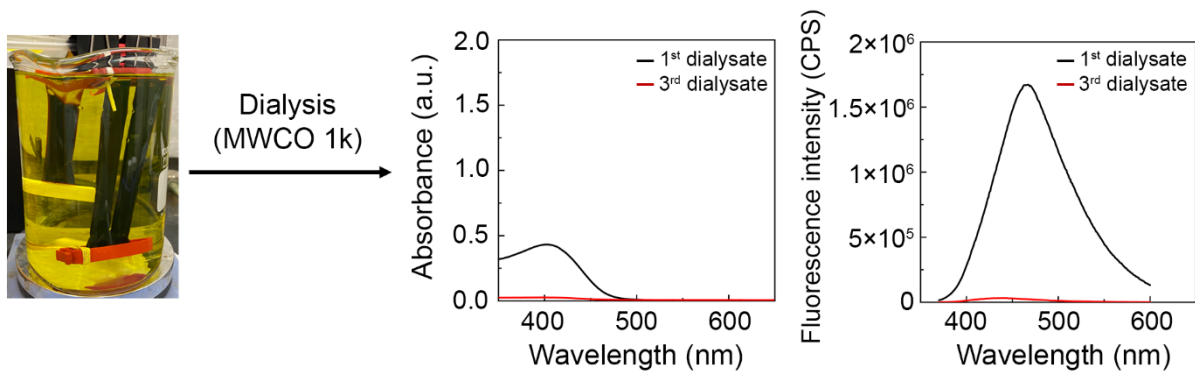


**Figure S1.** Removal of fluorescent by-products from synthesized CNDs. The CNDs were purified by dialysis until there was no significant absorbance or fluorescence of the dialysates.

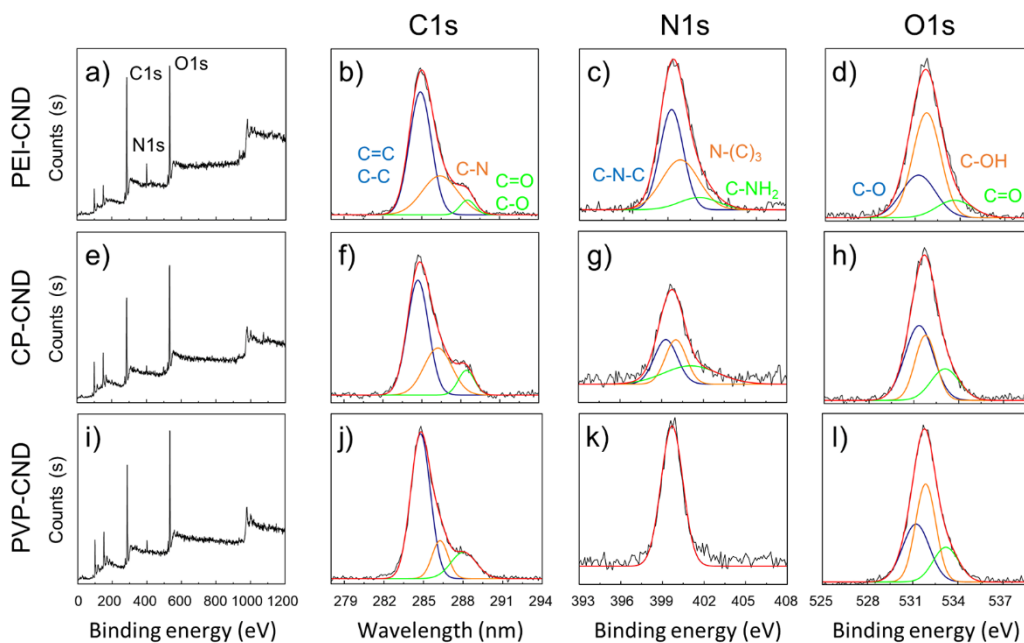


**Figure S2.** X-ray photoelectron spectroscopy (XPS) analysis of PEI- (polyethylenimine), CP- (carboxylated-PEI), and PVP- (polyvinylpyrrolidone) CNDs. Survey spectra of (a) PEI-, (e) CP-, and (i) PVP-CND. Panel (b-d), (f-h), and (j-l) represent high-resolution C1s, N1s, and O1s spectra of PEI-, CP-, and PVP-CNDs, respectively. All CNDs mainly consisted of C, N, and O atoms. The C1s XPS of PEI and CP-CND include graphitic C=C/C-C (284.8 eV), C-N (286.4 eV), and C=O or C-O (288.5 eV) bonds.<sup>2</sup> As expected, the PEI-CND showed a lower intensity of C=O bonds (288.5 eV) compared to CP-CND. The CP-CND exhibited an increase of C=O and C-O bonds due to the additional carboxylation groups. Furthermore, the N1s of PEI-CND had a higher intensity of C-N-C bonds relative to CP-CND. This XPS analysis indicates modification of amine functional groups in PEI-CND into carboxyl groups in CP-CND. The N1s spectra for both PEI- and CP-CNDs exhibited amine groups (C-NH<sub>2</sub>, 400 eV) but not for PVP-CND.<sup>3</sup> The PEI-CND contained more C-N-C bonds (399.2 eV) than CP or PVP-CND.<sup>4,5</sup> PVP-CND showed N1s peaks of C-N (399.7 eV) characteristic of PVP-coated nanomaterials.<sup>6,7</sup> Carbon nanodiamonds also contained C-O bonds such as C-O (531.2 eV), C-OH (531.9 eV), and C=O (533.2 eV)

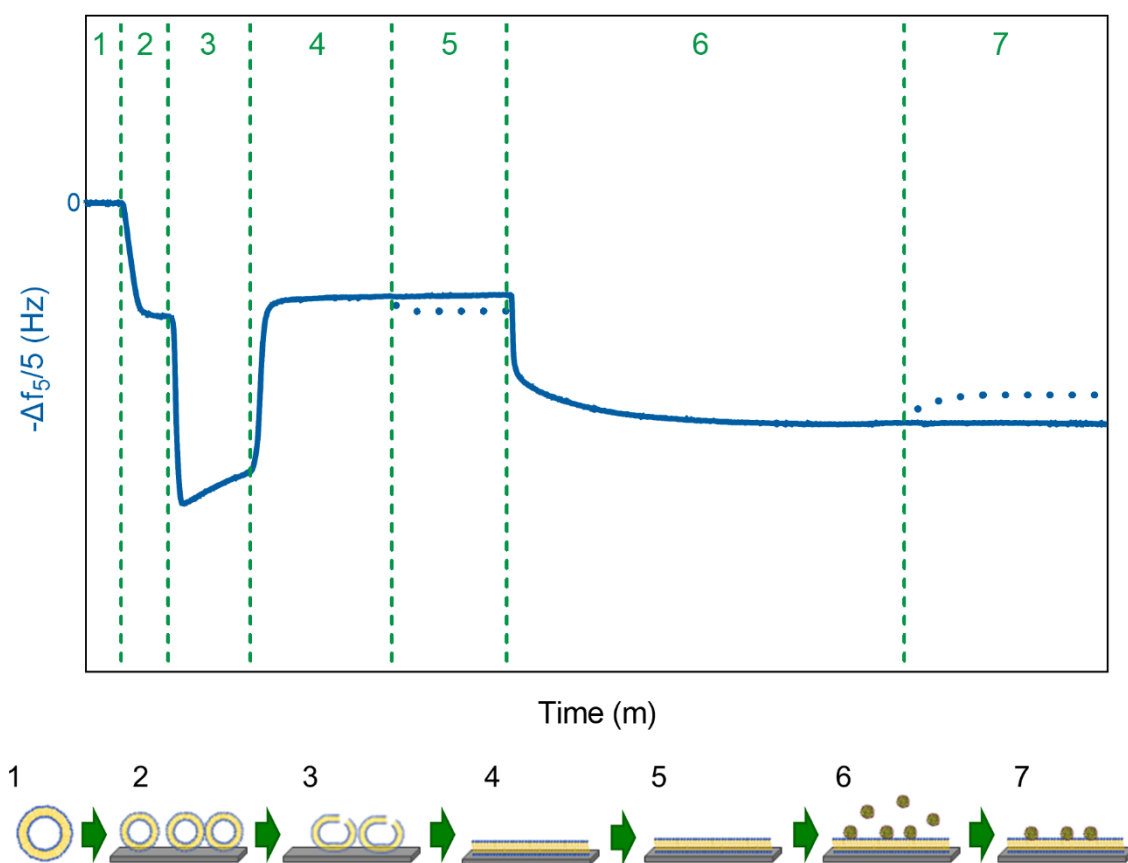


**Figure S3.** Formation of a representative 5 mol% SQDG containing bilayer and its interaction with positively charged CNDs in 10 mM KCl, 10 mM HEPES, pH 7.5 buffer. Salt conditions varied according to the bilayer formation process and testing conditions (Buffer composition below). The trace represents changes in the frequency of the 5<sup>th</sup> harmonic monitored by QCM-D. Prior to monitoring changes in acoustic mass densities, baseline was obtained in the lipid-free buffer flowing at a constant rate of 0.100 mL·min<sup>-1</sup> (Zone 1). Buffer flow rate was constantly maintained during the data acquisition. Once frequency signal is stabilized, we introduced a constant flow of vesicle solutions until frequency signal reached the plateau representing intact vesicle adsorption onto the sensor surfaces (Zone 2). To promote vesicle rupture and subsequent bilayer formation, we increased ionic strength of the buffer.<sup>8</sup> Adsorption of additional salt ions onto the surface led to a drastic decrease in frequency changes first, and vesicle rupture followed by the release of trapped water molecules caused an increase in the trace (Zone 3). When bilayer formation was completed and the traces were nearly stabilized, the formed bilayers were rinsed with the buffer that was used for the initial flow to remove residual vesicles or loosely bound lipid molecules from the surface (Zone 4). To investigate CND interactions with the model membranes under desired ionic conditions, we replaced the buffer with 0, 10, or 100 mM KCl containing buffers (Zone 5). Dotted line refers to changes in frequency under 100 mM KCl. Once we attained a stable frequency/mass plateau consistent with bilayer formation (Zone 5), the surfaces were exposed to a concentration of CNDs corresponding to UV absorbance of 1.2037 at 410 nm (Zone

6). Initial attachment efficiencies of each CND were determined in the early stage and we also obtained maximum acoustic mass densities on the bilayer in the latter stages of this zone. Once there were no significant changes in the traces, we rinsed the surface with the desired buffer to calculate the acoustic mass densities of CNDs that were tightly bound to the bilayers (Zone 7). The dotted line depicts detachment of weakly bound CNDs. All measurements were performed at a temperature of 25 °C. All solutions were buffered to pH 7.5 with 0.010 M HEPES and other components in buffers as follows:

Zone 1: 10 mM MgCl<sub>2</sub>

Zone 2: 0.125 mg·mL<sup>-1</sup> lipid vesicles and 10 mM MgCl<sub>2</sub>

Zone 3: 100 mM MgCl<sub>2</sub>

Zone 4: 10 mM MgCl<sub>2</sub>

Zone 5: 0, 10, or 100 mM KCl

Zone 6: CNDs and 0, 10, or 100 mM KCl

Zone 7: 0, 10, or 100 mM KCl

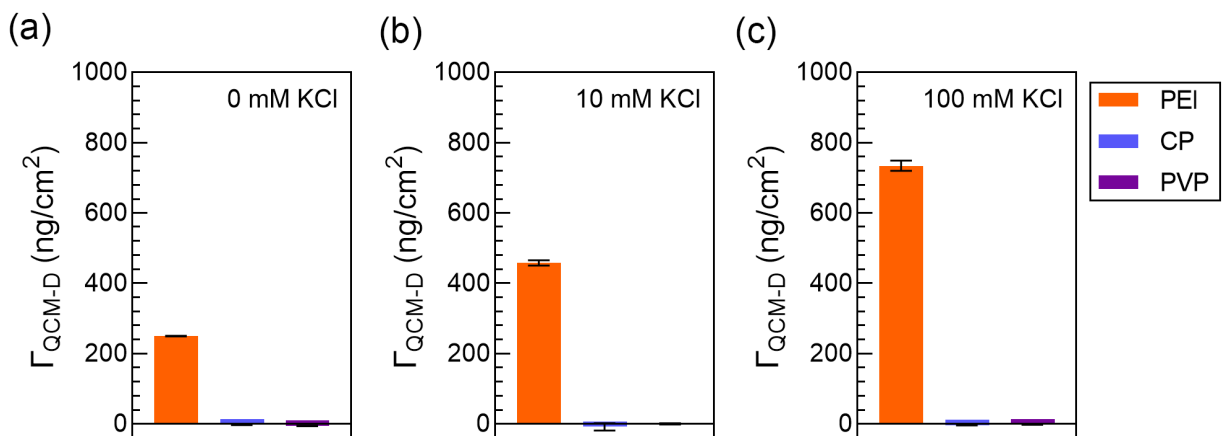


**Figure S4.** Changes in acoustic mass density ( $\Gamma_{\text{QCM-D}}$ ) upon interaction of PEI-, CP-, and PVP-CNDs with model membranes containing 5% SQDG in (a) 0, (b) 10, and (c) 100 mM KCl buffered to pH 7.5 with 10 mM HEPES. Error bars represent the standard deviation of triplicate measurements.

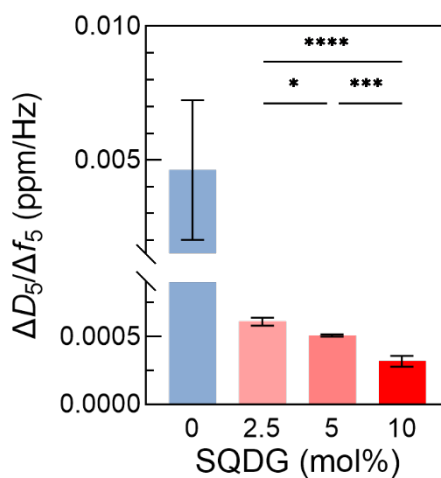


**Figure S5.** Calculated dissipation changes per unit adsorbed mass ( $\Delta D/\Delta f$ ) upon the interaction with the PEI-CNDs. The adsorption of PEI-CNDs induced decreasing propensity of  $\Delta D/\Delta f$ . Error bars represent the standard deviation of triplicate measurements. An analysis of variance followed by Tukey post-hoc tests revealed that each group is statistically different from the others. Significance of differences: \*,  $p \leq 0.05$ ; \*\*\*,  $p \leq 0.001$ ; \*\*\*\*,  $p \leq 0.0001$ .

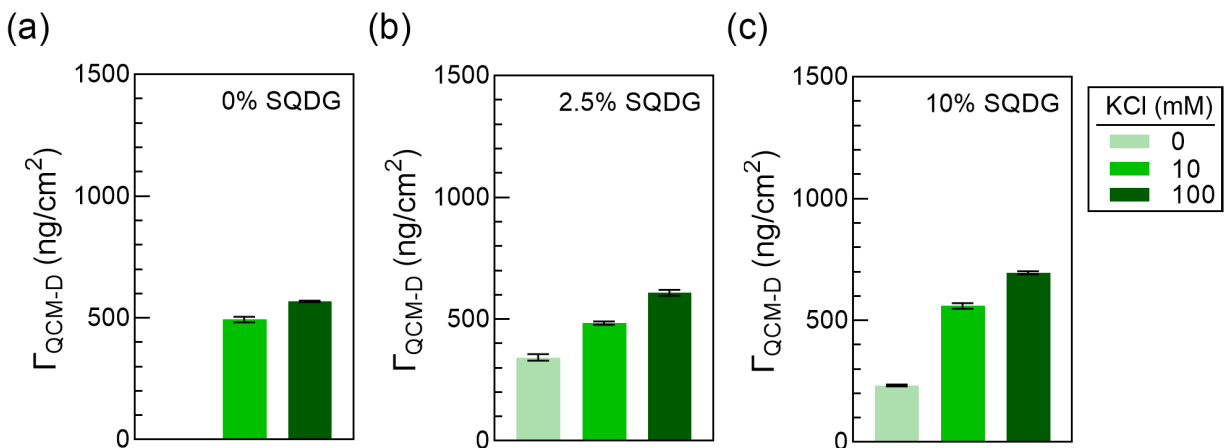


**Figure S6.** Mass densities upon PEI-CND exposure on (a) 0%, (b) 2.5%, and (c) 10% SQDG containing model membranes. Increase in KCl concentration led to rises of acoustic mass densities upon PEI-CND exposure. Error bars indicate the standard deviation of triplicate measurement.

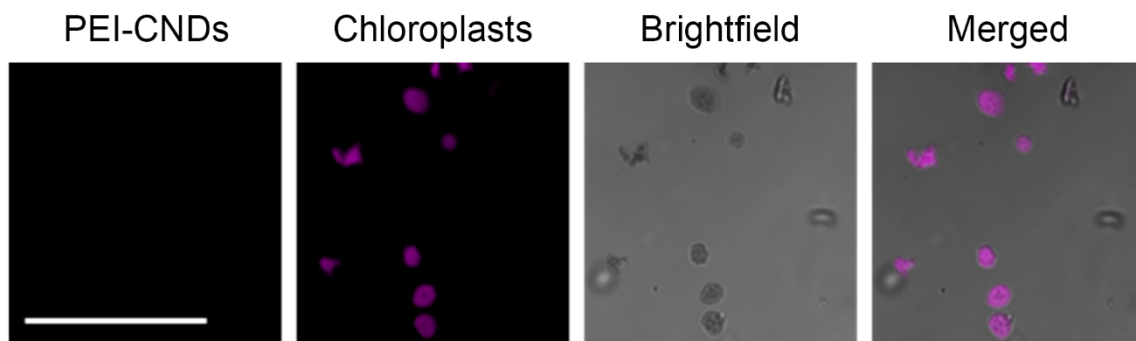


**Figure S7.** Representative confocal images of isolated chloroplasts without exposure to PEI-CNDs. Scale bar, 50  $\mu\text{m}$ .

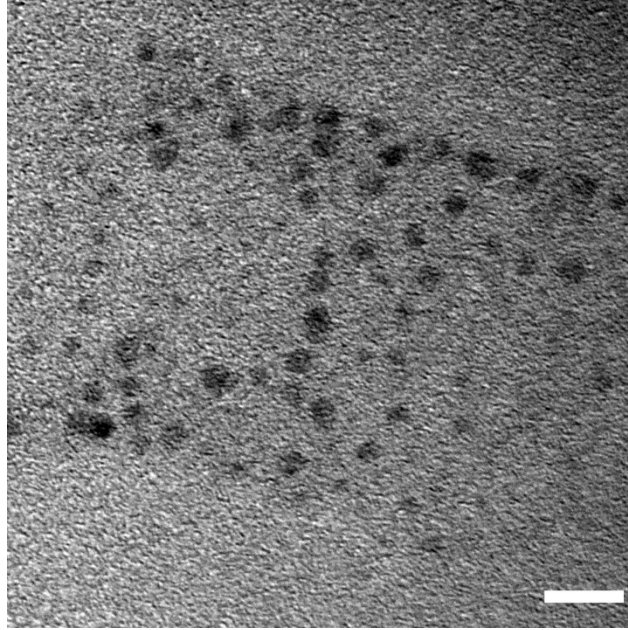


**Figure S8.** Representative TEM images of bare CNDs. Scale bar, 10 nm.

**Table S1.** Ratio of SQDG to PEI-CND at the maximum adsorption of CNDs

KCl (mM)	Density <sup>a</sup>	SQDG (mol%) <sup>b</sup>			
		0	2.5	5	10
0	Polypropylene	ND <sup>c</sup>	10 ± 0.4	25 ± 0.1	53 ± 0.8
	Diamond	ND <sup>c</sup>	39 ± 1.6	95 ± 0.5	201 ± 3.0
10	Polypropylene	6 ± 0.1	5 ± 0.1	12 ± 0.2	20 ± 0.4
	Diamond	23 ± 0.6	20 ± 0.3	46 ± 0.8	77 ± 1.6
100	Polypropylene	5 ± 0.0	56 ± 0.1	9 ± 0.2	19 ± 0.2
	Diamond	20 ± 0.1	21 ± 0.4	33 ± 0.7	71 ± 0.7

<sup>a</sup> Density of polypropylene and diamond: 0.92 g·cm<sup>-3</sup> and 3.53 g·cm<sup>-3</sup>, respectively

<sup>b</sup> We assumed, first, SQDG molecules were evenly distributed between outer and inner leaflet of model membranes, and second, all lipid molecules were involved in bilayer formation

<sup>c</sup> Not determined due to not detectable change in acoustic mass density

## REFERENCES

- (1) Jacobson, K. H.; Kuech, T. R.; Pedersen, J. A. Attachment of Pathogenic Prion Protein to Model Oxide Surfaces. *Environ. Sci. Technol.* **2013**, *47* (13), 6925–6934. <https://doi.org/10.1021/es3045899>.
- (2) Jeon, S.-J.; Kang, T.-W.; Ju, J.-M.; Kim, M.-J.; Park, J. H.; Raza, F.; Han, J.; Lee, H.-R.; Kim, J.-H. Modulating the Photocatalytic Activity of Graphene Quantum Dots via Atomic Tailoring for Highly Enhanced Photocatalysis under Visible Light. *Adv. Funct. Mater.* **2016**, *26* (45), 8211–8219. <https://doi.org/10.1002/adfm.201603803>.
- (3) Tang, J.; Zhang, J.; Zhang, Y.; Xiao, Y.; Shi, Y.; Chen, Y.; Ding, L.; Xu, W. Influence of Group Modification at the Edges of Carbon Quantum Dots on Fluorescent Emission. *Nanoscale Res. Lett.* **2019**, *14* (1). <https://doi.org/10.1186/s11671-019-3079-7>.
- (4) Wu, P.; Li, W.; Wu, Q.; Liu, Y.; Liu, S. Hydrothermal Synthesis of Nitrogen-Doped Carbon Quantum Dots from Microcrystalline Cellulose for the Detection of Fe<sup>3+</sup> Ions in an Acidic Environment. *RSC Adv.* **2017**, *7* (70), 44144–44153. <https://doi.org/10.1039/c7ra08400e>.
- (5) Hu, Q.; Wujcik, E. K.; Kellarakis, A.; Cyriac, J.; Gong, X. Carbon-Based Nanomaterials as Novel Nanosensors. *J. Nanomater.* **2017**, *2017*, 3643517. <https://doi.org/10.1155/2017/3643517>.
- (6) Safo, I. A.; Dosche, C.; Özaslan, M. Effects of Capping Agents on the Oxygen Reduction Reaction Activity and Shape Stability of Pt Nanocubes. *ChemPhysChem* **2019**, *20* (22), 3010–3023. <https://doi.org/10.1002/cphc.201900653>.
- (7) Jiang, P.; Zhou, J.-J.; Li, R.; Wang, Z.-L.; Xie, S.-S. Poly(Vinyl Pyrrolidone)-Capped Five-Fold Twinned Gold Particles with Sizes from Nanometres to Micrometres. *Nanotechnology* **2006**, *17* (14), 3533–3538. <https://doi.org/10.1088/0957-4484/17/14/029>.
- (8) Jackman, J. A.; Choi, J. H.; Zhdanov, V. P.; Cho, N. J. Influence of Osmotic Pressure on Adhesion of Lipid Vesicles to Solid Supports. *Langmuir* **2013**, *29* (36), 11375–11384. <https://doi.org/10.1021/la4017992>.